We are IntechOpen, the world's leading publisher of Open Access books Built by scientists, for scientists

4,800
Open access books available

122,000
International authors and editors

135M
Downloads

Our authors are among the

154
Countries delivered to

TOP 1%
most cited scientists

12.2%
Contributors from top 500 universities

CLARIVATE ANALYTICS BOOK CITATION INDEX INDEXED

WEB OF SCIENCE™

Selection of our books indexed in the Book Citation Index in Web of Science™ Core Collection (BKCI)

Interested in publishing with us?
Contact book.department@intechopen.com

Numbers displayed above are based on latest data collected.
For more information visit www.intechopen.com

16

Ablation of 2-6 Compounds with Low Power Pulses of YAG:Nd Laser

Maciej Oszwaldowski, Janusz Rzeszutek and Piotr Kuswik
Poznan University of Technology, Faculty of Technical Physics
Poland

1. Introduction

The 2-6 compounds and their mixed crystals are important semiconductor materials with practical applications in various areas of solid state electronics and optoelectronics. Most of the applications need these materials in a thin film form. One of the most versatile methods of obtaining thin films and their composed structures is the Pulsed Laser Deposition (PLD) method. That method has been used many times to the deposition of the 2-6 compound films and the result of the investigations of both the target ablation process and the obtained films physical properties were published in numerous publications. The earlier publications have been summarized in several excellent reviews (Cheung & Sankur, 1988; Christley & Hubler, 1994; Dubowski, 1991). In spite of the existing broad experimental material, optimum technological conditions for obtaining 2-6 compound layers by PLD with pre-defined properties has not as yet been determined. This is because the layers properties depend on the Pulsed Laser Ablation (PLA) process of the target material. The ablation depends on such parameters of the process as: the energy and duration of the laser pulse, pulse repetition frequency and the angle of incidence, target preparation method and some others. Therefore, the PLA is a multi-parameters process.

It has been recently shown (Rzeszutek et al., 2008a,b) that pulsed laser ablation of CdTe target with low - power pulses of YAG:Nd laser can be an effective method for the deposition of high quality CdTe thin films. The advantages of using low-power pulses of YAG:Nd laser for the CdTe ablation are following. The YAG:Nd laser is as such a very stable and environmentally harmless laser that can be very easy handled. Because the thermal evaporation of CdTe results in nearly congruent vaporisation of Cd and Te (Ignatowicz S. & A. Koblendza 1990), it may be expected that the low - power pulsed laser ablation should be a very effective method of the deposition of CdTe thin films. However, the most important reason that ablation is performed in the low-power regime, realized by long pulse duration of 100 μs, is to minimize the splashing effect that is the effect of emitting of macroscopic particularities from the target (Cheung & Sankur, 1988). That degrades the quality of the thin films obtained by the laser ablation. Therefore, the type of the laser and its pulse duration time are dictated by practical reasons.

In this chapter we summarize our earlier experiments on the ablation of CdTe and add new results on the ablation of CdSe and ZnTe not as yet published. Like CdTe, these two latter compounds, are rather volatile materials, and the use of the low-power YAG:Nd laser ablation for their thin film preparation can be substantiated largely in the same way as it is

done above for CdTe. Therefore, in the following we will present and discuss the results on the PLA of a group of the 2-6 compounds, which allows on some generalization of the conclusions.

However, our main goal is not the presentation of the physical properties of the 2-6 thin films obtained in the low-power regime of the YAG:Nd PLA. It is rather the ablation process itself and its dependence on the parameters of the process. Our main points of interest are: the dependence of the ablation process of the 2-6 compounds on the target preparation method and laser pulse energy and the effect of these factors on the velocity distribution of emitted particles.

The chapter's material is organized in the following way. In Sec. 2 the experimental procedures are described. Here a general experimental set-up for performing PLA is given together with the description of the Time-Of-Fly measurement method. Sec. 3 is devoted to the dependence of the pulsed laser ablation of the 2-6 compounds on target preparation method. In particular, the vapour stream intensity and the chemical composition and their mutual evolution with time are investigated with the help of a quadrupole mass spectrometer. These studies are performed for three kinds of targets: a target made of CdTe bulk crystal (BC target), a target made of CdTe fine powder pressed under the pressure of 700 atms (PP target), and a target made of loose (non-pressed) CdTe powder (N-PP target). Results obtained for PP targets made of CdSe and ZnTe are also presented. Sec. 4 deals with the velocity distribution of emitted particles. It starts with a theoretical background and continues with experimental velocity distribution of particles and comparison with the theory. The velocity distribution is determined by the time-of-fly (TOF) spectrometry performed by a quadrupole mass spectrometer. This section deals also with the angular distribution of particles. In Sec. 5 final conclusions are drawn.

2. Experimental procedures

2.1 Apparatus for pulsed laser ablation of semiconductor materials

The pulsed laser ablation of the 2-6 materials has been performed in an apparatus for pulsed laser deposition of semiconductor thin films described earlier (Oszwałdowski et al., 2003). A general scheme of the main part of the apparatus is shown in Fig. 1. Important elements of the apparatus are:

Laser. A typical neodymium doped yttrium–aluminum–garnet (YAG:Nd) laser is used. It has the following parameters: wavelength ,1.064 μm; maximum pulse energy, 0.5 J; instability of the pulse energy, 6%; pulse duration in the free generation mode, 100 μs; pulse duration in the *Q*-switched mode, 10 ns; repetition time, 10–50 Hz; beam divergence, 3 mrad; and beam diameter, 7 mm.

In the further described experiments the Nd:YAG laser operates at 25 Hz or 35 Hz pulse frequency. The pulse energy is changed from 0.13 J to 0.25 J; however most of the experiments are performed with the energy of 0.16 J. The laser spot on the target has the effective (roughly FWHM) diameter of 0.2 cm, thus the surface density of the energy is changed from 4 J/cm^2 to 8 J/cm^2, and the most frequently applied energy density is 5 J/cm^2. For the applied laser pulse duration of 100 μs, the pulse power is changed from $1.3 \cdot 10^3$ W to $2.5 \cdot 10^3$ W, and the most frequently applied power is $1.6 \cdot 10^3$ W. Therefore, the applied laser pulse powers fall into the low power regime (Cheung &.Sankur, 1988; Christley &Hubler, 1994). The low pulse power and the relatively large laser spot are chosen to diminish the splashing.

Optical path of laser beam. The laser radiation beam falls onto a focusing mirror having the focal length of 80 cm. This mirror is attached to a guide that enables to shift the mirror, and thereby its focal point in relation to the targets plane. As a rule, in order to decrease the radiation surface density power with the aim of avoiding splashing, the mirror focal plane is shifted from the target plane. The extent of the off focusing depends on the target material.

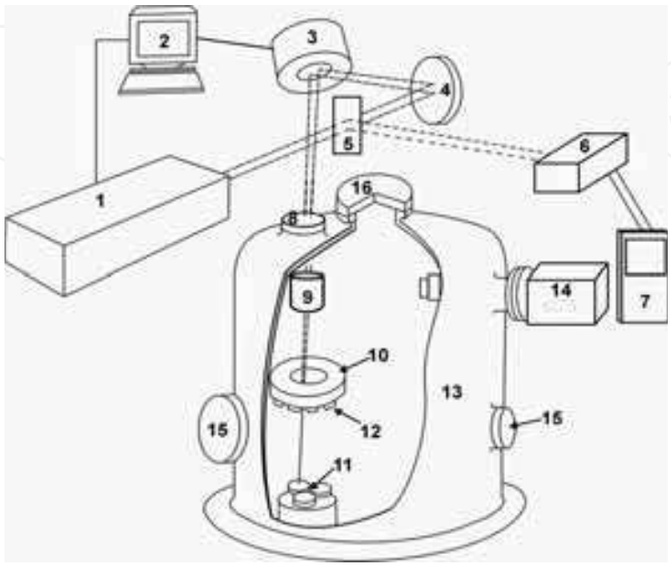

Fig. 1. Sketch of the apparatus for PLD of semiconductor thin films.
1. YAG:Nd laser, 2. Computer controlled system of laser beam monitoring, 3. Device switching laser beam between targets (optical deflector) , 4. Focusing mirror, 5. Quartz plate, 6. Photodiode system for measurement laser beam intensity, 7. Meter or oscilloscope, 8. Optical port of laser beam, 9. Heater of internal optical port, 10. Substrate holder and heater, 11. targets, 12. Substrates, 13. Vacuum chamber, 14. QMS at first port, 15. Peep holes, 16. Second QMS port.

The concave mirror reflects the beam onto a flat mirror of the optical deflector, which directs the beam through an opening in the substrate holder/heater onto a surface of one of the targets.
Other details of the apparatus construction less important for the present studies can be found in the source article (Oszwałdowski et al., 2003)
Quadrupol Mass Spectrometer (QMS) The apparatus is supplied with a quadrupole mass spectrometer (QMS, HALO 301, Hiden Analytical) equipped with a pulse ion counter. The action of the QMS is synchronized with the laser action by a specially designed electronic device. With this improvement, the vapour cloud ejected from the target by a laser pulse arrives at the spectrometer head in a proper time to be recorded and analysed on its chemical composition. Determination of chemical composition of the vapour stream and the velocity distribution of emitted particles are main functions of QMS in present investigations.

2.2 Time-Of-Fly experiments

An important part of the present investigations is performed with Time-Of-Fly (TOF) experiments. They are carried out with the use of the quadrupole mass spectrometer

equipped with a pulse ion counter (PIC) as an ion detector. Here, the option of the measurements of the delay times between the electric pulse triggering the laser shot and the detection of the ionized particles by the ion detector is exploited for the determination of the particle delay time distribution (Rzeszutek et al., 2008b). From that, the velocity distribution of particles in the vapour stream is determined. The total particle delay time is composed of the following partial delay times: the laser pulse generation time, the particle emission time, the particle TOF between the target and the orifice of the ionizer, the particle arrival to PIC time, the PIC reaction time (given by the manufacturer to be between 30 ns and 50 ns). The time of the laser pulse generation is determined with the help of an electronic circuit equipped with a photodiode as a radiation detector. The time of the laser pulse generation is assumed to be the FWHM of the signal shown, which is about of 70 μs, and thus is close to the value of the 100 μm given by the QMS manufacturer.

The sketch of the configuration applied in the measurement of TOF is shown in Fig. 2. The TOFs are measured with the substrate heater, *H* removed from its position (10) in the vacuum chamber shown in Fig. 1. The sum of the remaining delay times is determined from the difference in the total delay times t_1 and t_2, measured at two different distances l_1 = 43 cm and l_2 = 24 cm between the target and the ionizer entry. For this purpose, the particle velocity $v = (l_1\text{-}l_2)/(t_1\text{-}t_2)$ was determined in the first step. Then, from the knowledge of v, t_1 and t_2 the sum of the remaining delay times is determined to be 0.12 ms. In the subsequent measurements, the TOFs were measured only for the distance l_1 and the TOF velocity was determined from the equation: $v = l_1 / (t_1 - 0.12)$, where t_1 is in milliseconds. The measured values of $(t_1 - 0.12)$ were in the range from 0.4 to 4 ms, whereas the range of measurable delay times was from 0.1 to 100 ms. Thus, the system was capable to measure the TOFs of all particles that appeared at the ionizer.

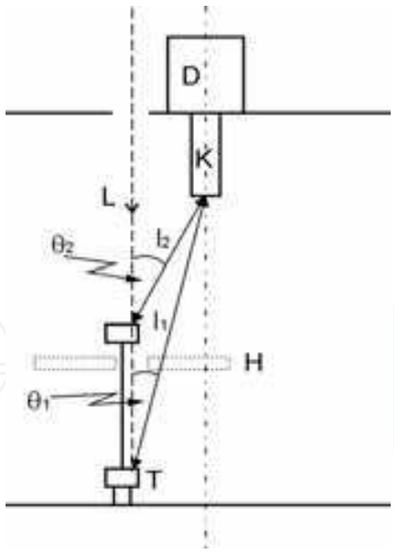

Fig. 2. Sketch of configuration applied for TOF and angular distribution measurements. (*D*) particle detector (PIC), (*K*) particle ionizer and quadrupole, (*T*) target, (*L*) laser beam, l_1 & l_2 distances between lower and upper position of target, respectively, (*H*) substrate heater, removed from position for TOF measurements.

The target holder is a rotating copper cup having the inner diameter ϕ = 2 cm. The angular velocity of the cup can be changed.

2.3 Target preparation method

In the present experiments three types of targets are used: a target made of powdered material poured directly into the holder cup (non-pressed powder target, N-PP target), a pellet made of a fine powder pressed at a pressure of 700 atm (pressed powder target, PP target), and a slice cut off from a CdTe bulk crystal (bulk crystal target, BC target). The diameter of the targets made of the powder is 2 cm and the diameter of the bulk CdTe crystal target is 1 cm. The ablation runs, lasting 9-14 minutes are performed at a constant laser power. The quadrupole system of the QMS head is directed roughly towards the target. The orifice of the head is lightly shifted parallel to the target surface in such a way that the line joining the orifice centre with the target centre makes an angle of 19° with the target normal. The distance between the orifice and the target surface is 43 cm. During the ablation process the pressure in the vacuum chamber is about 10^{-6} torr.

3. Pulsed laser ablation of 2-6 compounds: Dependence on target preparation method

3.1 Dependence of vapour stream intensity on pulse

The study of the dependence of the vaporisation intensity of CdTe, CdSe and ZnTe on the laser pulse energy is performed on the PP targets. The vapour stream intensity for each compound is deduced from two different and independent measurements. In the first measurement method total amount of the mass ablated by the action of 10000 laser pulses of a given energy is measured by weighing the pellet before and after the ablation and evaluating the difference. From these data the average mass ablated by a single pulse is determined. In the second measurement method, the total number of counts is registered, by the QMS, in the same ablation process for the isotope ^{110}Cd in the case of CdTe and CdSe and the isotope ^{66}Zn in the case of ZnTe. From that, the average number of counts for a single pulse is determined. Thus, in both measurements, a magnitude proportional to the vapour stream density is determined. The measurement results for the laser pulse energies ranging from 130 mJ to 250 mJ are shown in Fig. 3.

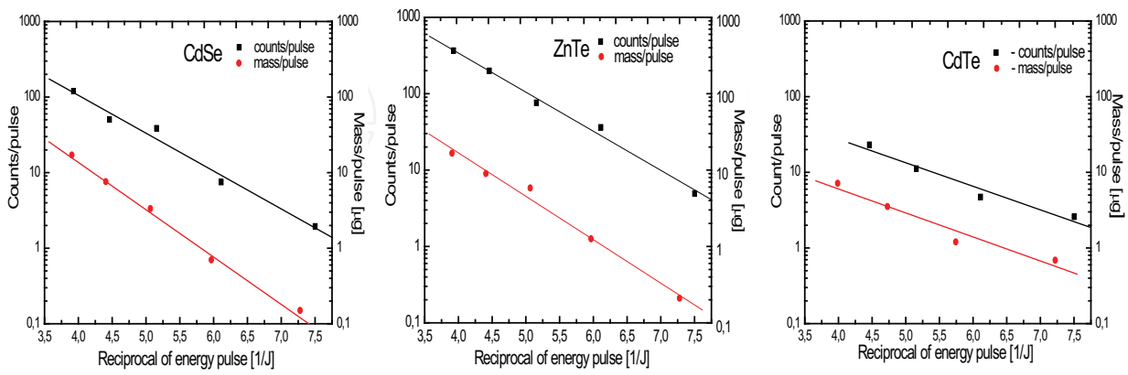

Fig. 3. Dependence of the vapour stream intensity from CdSe, ZnTe and CdTe PP targets on the inverse of the laser pulse energy ranging from 130 mJ to 250 mJ. The left scale shows the number of QMS counts per a single laser shot. The right scale shows the mass ablated by a single laser shot

It is seen in the figure that for both measurement methods, there is a good agreement as for the character of the dependence of the vaporisation intensity on the pulse energy. This dependence is linear in the scale logarithm of the vapour stream density versus the inverse of the pulse energy. In the applied range of the energy density, the mass evaporated by a single laser shot is between 0.6 μg and 8 μg for CdTe, and between 0.1 μg and 20 μg for CdSe and ZnTe. Thus the effectiveness of evaporation for CdSe and ZnTe is higher.

The presented studies of the dependence of the vapour stream density on pulse energy for the targets made of CdTe, CdSe and ZnTe are performed in the power density range (4-8)*10^4 W/cm^2 that is for the densities smaller than 10^6 W/cm^2, which is a region known as the low power density range (Cheung & Sankur, 1988). In this range the particle emission is expected to have the thermal character, in which the stream density S depends on the thermal energy kT, acquired from the pulse energy E according to the relationship:

$$S \propto \exp\left(-\frac{\Delta H}{kT}\right) \tag{1}$$

where ΔH is the heat of vaporisation. Fig. 3 shows that the results for the PP targets comply with Eq. (1) under the assumption that the kT is proportional to the pulse energy. However, it should be pointed out that in the case of materials having a high vapour pressure, the ablation with laser pulses in the low power density regime does not mean a low particle stream density (Kelly & Miotello, 1994).

Since CdTe, CdSe and ZnTe show in Fig. 3 a linear dependence of the stream density on the energy pulse reciprocal, it is possible to calculate the slopes of the curves. They should be roughly proportional to the heats of vaporisation (enthalpies of sublimation). The determined curve slopes for CdSe, ZnTe and CdTe respectively are: -1.33 μg J/pulse, -1.24 μg J/pulse and -0.78 μg J/pulse. The respective enthalpies of sublimation for CdSe, ZnTe and CdTe are: 1.7 10^6 J/kg (Bardi et al., 1988), 1.6 10^6 J/kg (Nasar & Shamsuddin, 1990) and 1.2 10^6 J/kg (Bardi et al., 1988). Comparing the absolute values of the curve slopes with the values of the enthalpies of sublimation, we find some correlation between them. Namely, they decrease in the same order and the values for CdSe and ZnTe are very close, whereas corresponding values for CdTe are distinctly smaller. The correspondence between the curve slopes and the sublimation enthalpies seems to further confirm the thermal nature of the ablation process.

Each change in the pulse energy has an effect on the surface appearance of the ablated area. A similar effect has the degree of the spatial overlapping of two consecutive laser shots on the target. The surface appearance of a PP target made of CdTe and ablated with laser shots having the energy of 160 mJ is shown in Fig. 4. The shown in the figure detail is a fragment of a 2 mm wide circular track carved by the laser beam on the target surface. The left-hand side of the figure marked a) shows an area ablated with 20000 laser shots, of which spots did not overlapped. After moving the laser spot along the target radius towards the target centre and reducing the angular speed of the target to a half of its initial value, the consecutive laser spots overlapped. The result of the ablation performed with overlapping spots is shown on the right-hand side of the figure, marked b). The left- and the right-hand side of the figure are separated by a narrow and smooth part of the target surface, marked c) that was not laser ablated. It is seen in the figure that the laser ablation results in formation of a surface structure consisting of granular forms. However, the topography of the part

ablated with the overlapping spots is richer and shows higher roughness. The ablation with overlapping spots increases local temperature of the ablated area formed by 2-3 consecutive shots. This effect, called further overheating, is equivalent to the increase in the energy of the laser pulse.
The effect of a genuine increase of the laser pulse energy is shown in Fig. 5.

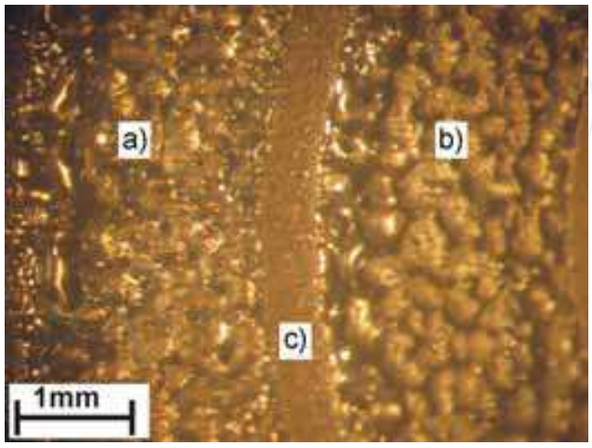

Fig. 4. Surface appearance of CdTe PP target ablated with 160 mJ laser pulses (optical microscope).
Part a) shows fragment of circular track ablated with 20000 non-overlapping laser shots. Part b) shows fragment of circular track ablated with 20000 overlapping laser shots. Both parts are separated by narrow circular strip (c) of the material that was not laser ablated.

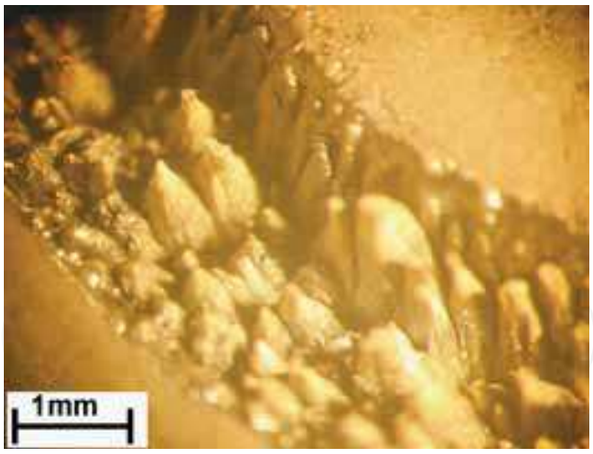

Fig. 5. Surface appearance of CdTe PP target ablated with 250 mJ laser pulses (optical microscope). Surface structure is obtained after 30000 laser shots.

The observed fragment of the circular track is a result of the ablation with non-overlapping shots, 30000 in number, with the pulse energy of 250 mJ. Comparing Fig. 4 and Fig. 5, it can be seen that the increase in the shot energy leads to a more developed surface structure showing considerably higher roughness. This is quite a general observation for all studied materials, as may be concluded from Fig. 6 that shows the results for CdSe and ZnTe PP targets.

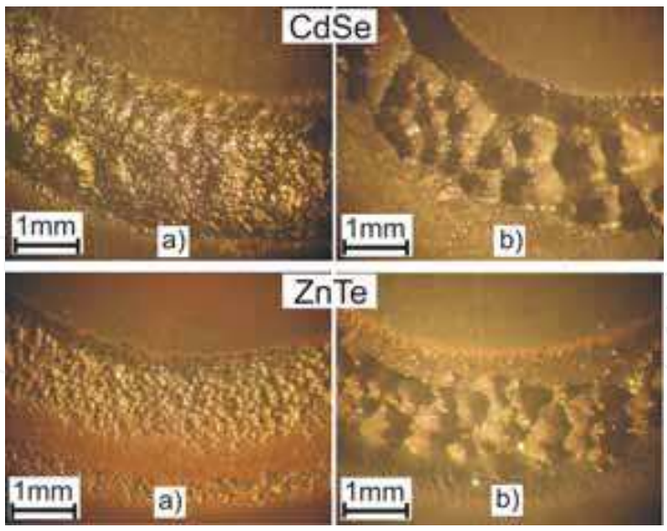

Fig. 6. Surface morphology of CdSe and ZnTe PP targets after ablation with laser pulse energy: 130 mJ, a) and 250 mJ, b).

It is clearly seen that the fragments of the targets ablated with the 130 mJ pulses is much smoother that the fragments ablated with the 250 mJ pulses. In Figs 4, 5, and 6 one can observe than at the higher pulse energy (250 mJ) the formation of characteristic conical forms occurs in the ablated material. This formation can be associated with the granular nature of the PP targets.

3.2 Vapour chemical composition and its time dependence

In order to perform the stream intensity measurements with QMS, it is necessary to choose a proper isotope of each element of the compounds. The number of isotopes of Cd, Zn, Se and Te respectively is: 8, 5, 6 and 7. For the monatomic species we have chosen the following isotopes: ^{110}Cd, ^{66}Zn, ^{78}Se, and ^{128}Te. For the diatomic species we have chosen: $^{256}Te_2$ resulting from the sum (pairing) of the monatomic species: ^{128}Te + ^{128}Te and ^{126}Te + ^{130}Te. For $^{156}Se_2$ we have chosen resulting from the sum of the monatomic species: ^{78}Se + ^{78}Se, ^{76}Se + ^{80}Se, ^{74}Se + ^{83}Se. This choice of the masses is an optimum from the point of view of the measurement convenience. With this choice, the QMS signals from all the chosen masses have comparable amplitudes. That enables their convenient observation on the screen in the same signal scale.

In the case of CdTe, all three forms of the target are investigated. Prior to the investigations of the vapour streams generated by the laser, we studied the vaporisation of CdTe powder by the normal thermal vaporisation from a heated quartz crucible. We were particularly interested in the ratio of the vapour streams of the monatomic and the diatomic forms, $J(Te)/J(Te_2)$. In the investigations we have found that at relatively slow thermal vaporisation of CdTe powder, the ratio of the QMS signals from the masses 128 and 256 is 0.25 and shows tendency to increase to about 0.5 at a fast vaporisation. Hence, taking into account the species abundances we obtained that purely thermal evaporation of CdTe gives at least a 20 % participation of monatomic Te in the stream.

The investigations of the chemical composition of the vapour stream generated by the laser pulses are performed both with overlapping and non-overlapping laser shots. The ablations are carried out with 160 mJ pulses and the frequency of 35 Hz. A typical ablation time is 9

minutes, and that corresponds to 20000 laser pulses. Results obtained for the BC target are shown in Fig. 7. Results obtained for non-overlapping spots are shown in the left-hand side panels, and those for overlapping laser shots are shown in the right-hand side panels. The panels a1 and a2 show the time dependence of the QMS signals from the ^{110}Cd and the ^{128}Te isotopes as well as for the $^{256}Te_2$ molecules.

It should be noted that the particle emission starts with some delay, which amounts to about one minute, counting from the beginning of the ablation. Such a delay for the start of the ablation was also observed in earlier works for various target materials. In the case of CdTe it was explained by the existence of an energy threshold for the ablation. The existence of the threshold was explained with a complicated mechanism, in which a two-phonon mechanism is employed at the initial stage to heat-up the material to the level sufficient for the generation of numerous structural defects and a decrease in the energy gap that enable much more effective single-phonon absorption in the final stage (Dubowski, 1991). At that moment the target material shows very high absorption for the laser radiation.

Comparing the dependences shown in the panels a1 and a2, it is seen that the stream intensity at the beginning of the ablation is higher for the ablation with overlapping spots, but it decreases considerably with time. No such a decrease is observed for the non-overlapping spots. The higher stream intensity observed for the ablation with the overlapping spots is clearly due to the higher local temperature at the spot area that results from a cumulative heat effect of the overlapping laser shots. This is an outcome of the poor heat conductivity of CdTe.

It may be seen in the panels a1 and a2 of Fig, 7 that the time dependence of the stream intensity for all masses has the same character, except for the first two minutes. This means that after the first two minutes the masses are emitted from the target congruently.

To make it more clear, we determine the time dependence of the relative signal intensities $S(^{110}Cd)/S(^{256}Te_2)$ and $S(^{110}Cd)/S(^{128}Te)$ from the data shown in the panels a1 and a2. The results are shown in the panels b and c respectively. It is seen that if the first two minutes are skipped, the signal ratios do not show any clearly marked dependence on time. That means that the total vapour stream has stoichiometric composition corresponding to the CdTe compound. It is also observed in Fig. 7 that the signal ratio $S(^{128}Te)/S(^{256}Te_2)$ increases with time during the first two minutes from the value of about 1.5 to the value of about 2.5, and then tends to saturate at this value. Taking into account the particle abundances (Rzeszutek et. al., 2008a), it results that the total particle stream ratio $J(Te)/J(Te_2)$ increases from 1.2 to 2.0. The latter value is by about an order of magnitude higher than the 0.25 obtained for the pure thermal evaporation. Therefore, in the case of the bulk crystal target and the ablation without the laser spot overlapping, the vapour stream contains twice more monatomic Te particles than diatomic Te_2 particles. This is quite different from the case of the same target, but ablated with the laser spot overlapping. As seen in the panel b2, in that case the signal ratio $S(^{128}Te)/S(^{256}Te_2) = 0.5$, and it is constant from the beginning of the ablation. The value 0.5 corresponds to the particle stream ratio $J(Te)/J(Te_2)$ amounting to 0.41 and, as mentioned earlier, this is also the value characteristic for a fast thermal evaporation at high temperatures.

The panels c1 and c2 of Fig. 7 show that the signal ratio $S(^{110}Cd)/S(^{128}Te)$ decreases during the first two minutes of the ablation, and then saturates. It is clear that in the case of the non-overlapping laser shots, this initial decrease is in fact due to a relatively smaller participation

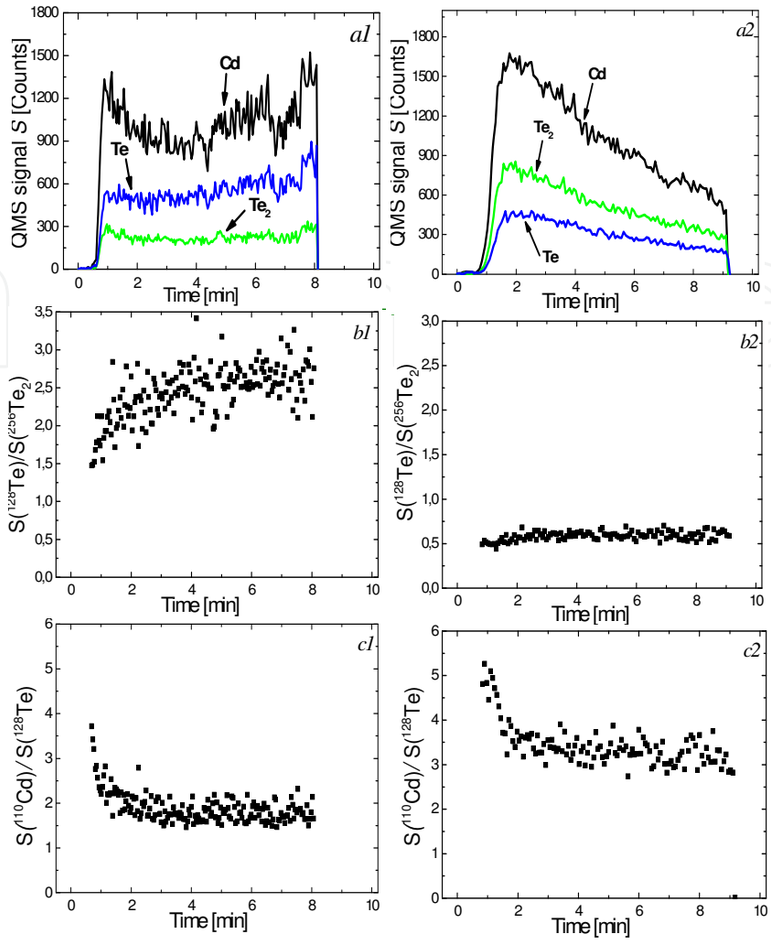

Fig. 7. Time dependence of QMS signals obtained during laser ablation of CdTe BC target. Left panels show dependence for non-overlapping laser shots, and right panels show dependence for overlapping laser shots. Panels a1 and a2 show time dependence of QMS signals from Cd, Te and Te_2. Symbols $S(^{128}Te)/S(^{256}Te_2)$ or $S(^{110}Cd)/S(^{128}Te)$ in remaining panels mean ratio of signals S from Te and Te_2 or from Cd and Te respectively. Ablation is performed with laser frequency of 35 Hz and pulse energy of 160 mJ.

of the monatomic Te species in comparison with the diatomic Te_2 species in the total tellurium stream (panel b1). The time dependence of the ratio $S(^{110}Cd)/S(^{256}Te_2)$ (not shown) does not reveal any such a decrease. On contrary, in the case of the overlapping laser shots, that initial decrease, as may be concluded from the panel b2, cannot be associated with any change in the participation of the monatomic Te species in the total tellurium stream. Thus, the initial decrease is associated with an initial excess of cadmium in the vapour stream.

Investigations of the ablation process of the PP targets are performed in the way analogous to those described for the bulk CdTe target. These investigations reveal that at the same ablation conditions the erosion of the target made of pressed power is considerably larger than that of the BC target. Since the initial smoothness of both types of the targets was similar, this may confirm that the much larger roughness of the pressed powder target is associated with its granular character. The investigation results for the CdTe PP targets are shown in Fig. 8.

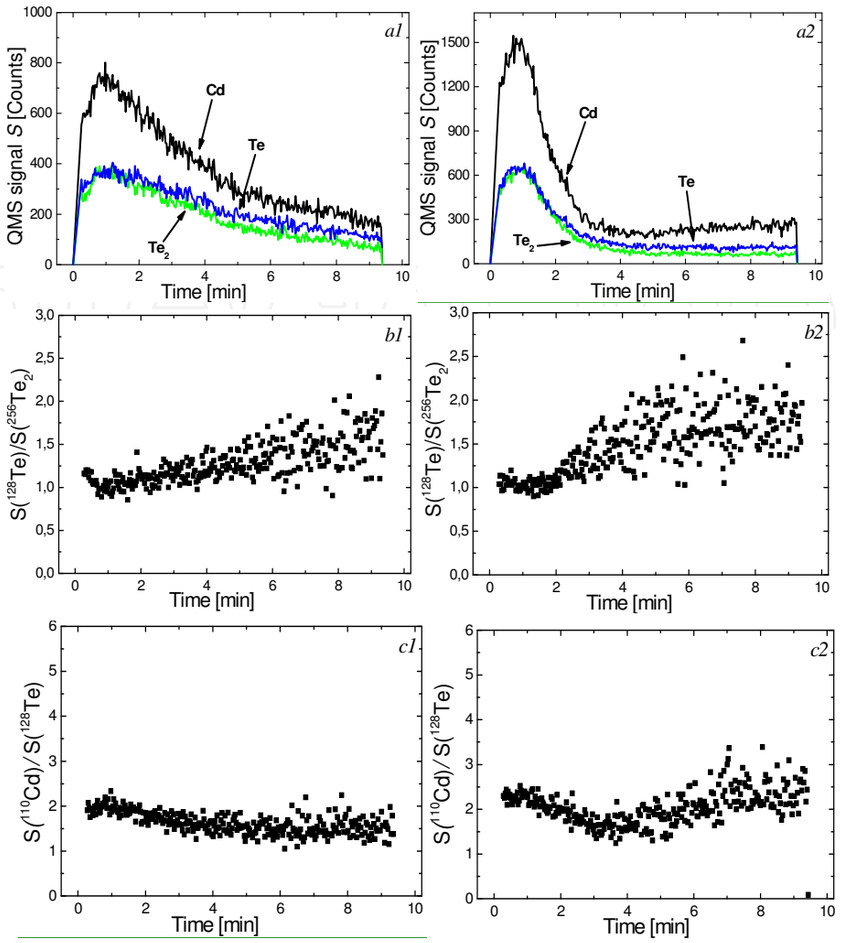

Fig. 8. Time dependence of QMS signal obtained during laser ablation of CdTe PP target. Left panels show dependence for non-overlapping laser spots, and right panels show dependence for overlapping laser spots. Panels a1 and a2 show time dependence of QMS signals from Cd, Te and Te_2.. Symbols $S(^{128}Te)/S(^{256}Te_2)$ or $S(^{110}Cd)/S(^{128}Te)$ in remaining panels, mean ratio of signals S from Te and Te_2 or from Cd and Te respectively. Ablation is performed with laser frequency of 35 Hz and pulse energy of 160 mJ.

It is seen in the panels a1 and a2 that in contrast to the BC target, in the present case the particle emission process commences immediately after the start of the laser action. This means that the powdered CdTe has sufficiently large number of structural defect to be strongly absorbent for the laser radiation. In the case of the non-overlapping laser spots, the magnitude of the QMS signal is slightly lower at the ablation beginning, as compared to the signal magnitude from the bulk crystal CdTe target, and further decreases with time. On the other hand, in the case of the overlapping laser spots, the magnitude of the QMS signal is comparable with that from the bulk crystal CdTe target at the ablation beginning, but its further decrease with time is stronger. Comparing the results for the overlapping and non-overlapping spots in the panels a1 and a2 of Fig.8, it is seen that the signal decrease is distinctly stronger in the case of the overlapping spots. In contrast to the ablation of the bulk crystal CdTe target, in the present case during the first 1-2 minutes of the intense particle emission, sporadic splashing is observed. Approximately after that time, a crust is formed

on the ablated surface of the target. The crust is located in a groove formed by the laser action. At that time, the target surface becomes increasingly rough. The crust is expected to be formed in the process of melting and subsequent freezing of the powder.

Panels b1 and b2 in Fig. 8 show the ratio of the signals for the masses 128 and 256. During the first 1-2 minutes this ratio is roughly constant, and next it increases with the ablation time from the value of 1 to about 1.7. These values correspond to the vapour stream ratio J(Te)/J(Te_2) from 0.82 to 1.4. The signal ratio S(^{110}Cd)/S(^{128}Te) slightly decreases during the first three minutes of the ablation, and then slightly increases with time. This behaviour is more clearly seen in the case of the overlapping laser spots (panel c2). The increase with time and simultaneous increase in the S(^{128}Te)/S($^{256}Te_2$) ratio can be understood under the assumption that in addition to the direct laser ablation, there is also a contribution from purely thermal evaporation of the target material associated with its local overheating resulting from the low thermal conductivity of the pressed powder. In such a case, one could expect the thermal evaporation component would show an excess of cadmium. This assumption is supported by the fact that the increase in the ratio S(^{110}Cd)/S(^{128}Te) is more pronounced in the case of the overlapping laser shots, which cause a larger overheating.

The characteristic features of the ablation process of the N-PP target can be presented by a comparison of the experimental results obtained for the N-PP target with those obtained for the BC and the PP targets. In the case of the N-PP target, the signal magnitudes both for the ablation with and without overlapping of the laser shots are markedly higher than those for the PP target, and also higher than those for the BC target. During the ablation of an N-PP target splashing is observed and that is particularly intense during the first 1-2 minutes. Moreover, during the ablation, a glowing tail is formed and it follows the laser spot in its travel around the moving target. The glowing part of the target has to be the source of purely thermal evaporation of the target material. Like in the case of the BC and PP targets, the ablation with overlapping laser shots is more effective. In comparison with the PP target, the decrease with time of the stream intensity is markedly smaller, and resembles that occurring for the bulk crystal target, however, with the exception that the particle emission starts immediately after the laser action onset. The composition of the tellurium vapour stream is dominated by the thermal evaporation from the glowing spot (Rzeszutek et al., 2008a).

As in the case of the PP target, the laser ablation leads to the formation of a crust on the top of the ablated powder. The ablated surface roughness of the N-PP target is considerably higher than that of the PP target. Also the laser carved groove is considerably deeper.

The investigations of the chemical composition of the vapour stream for ZnTe and CdSe are performed on pressed powder targets. The ablations are carried out with 25 Hz pulses in time of 9 minutes that corresponds to about 10000 laser pulses. The pulse energy is 250 mJ for CdSe, and 220 mJ for ZnTe. Results obtained for ZnTe are shown in the left-hand side panels, and those for CdSe are shown in the right-hand side panels of Fig. 9.

Panel a1 shows the time dependence of the QMS signals from ^{66}Zn and ^{128}Te isotopes as well as from $^{256}Te_2$ molecules. On the other side, panel a2 shows the time dependence of the QMS signals from ^{110}Cd and ^{78}Se isotopes and from $^{156}Se_2$ molecules. It may be observed in both panels that at an initial stage of the ablation, the signal intensity increases. This may be associated with gradual heating up the target by the laser action. If this is the case, comparison of Figs. 7 and 9 leads to the conclusion that the heating up is much faster for CdTe than that for ZnTe. The reason for that is unknown.

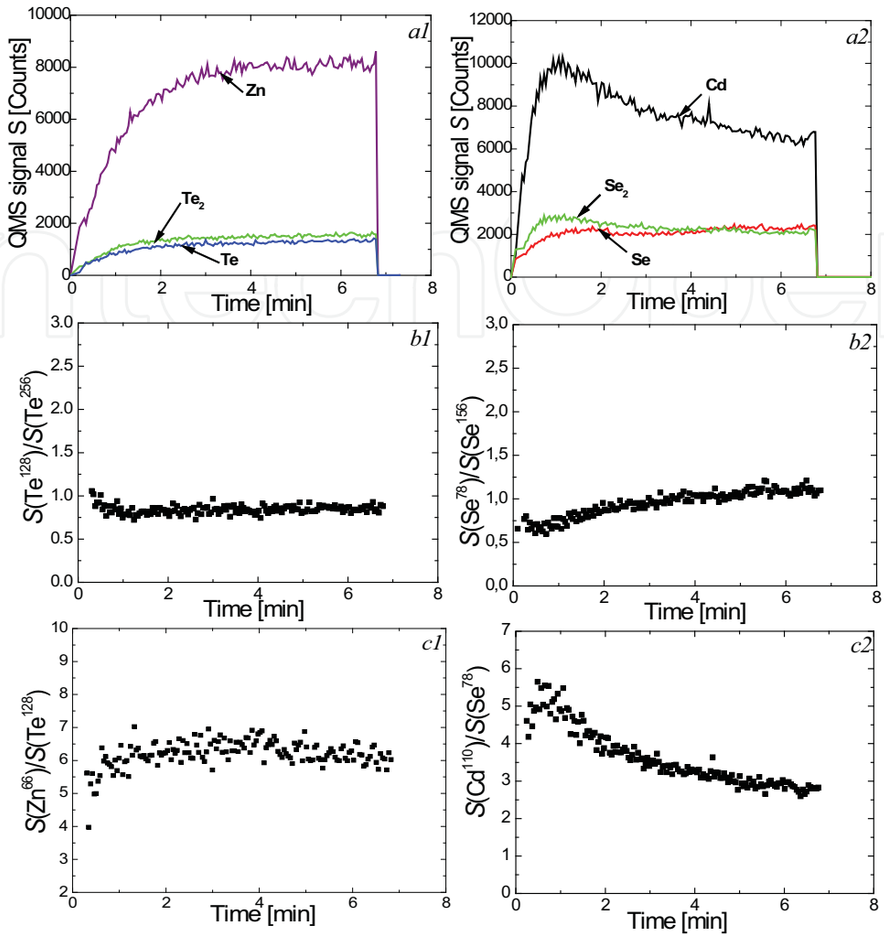

Fig. 9. Time dependence of QMS signal obtained during laser ablation of PP targets made of ZnTe, left panels and CdSe, right panels. Panel a1 shows time dependence of QMS signals from Cd, Te and Te_2, and panel a2 shows time dependence of QMS signals from Cd, Se and Se_2. In remaining panels are shown ratios of signals S from various particle streams. Ablations are performed with laser non-overlapping spots, frequency of 25 Hz and pulse energy of 220 mJ, for ZnTe, and 250 mJ, for CdTe.

Panels a1 and a2 show also that time dependences of the signals from all masses are more or less the same. A more precise investigation of this observation can be done by the determination of the ratios of signals from various masses. This is done in further panels. Panel b1 shows the time dependence of the ratio of the signals from the masses 128 and 256, and panel b2 shows the time dependence of the ratio of the signals from the masses 156 and 78. As it is seen, with the exception for the initial stage of the ablation, both ratios are time independent in the first approximation. It is interesting that the signal ratio $S(^{128}Te)/S(^{256}Te)$ is close to unity and weakly time dependent both for ZnTe and CdTe (Fig. 7). Thus the signal ratio is weakly dependent of the chemical composition.

Panel c1 shows the time dependence of the ratio of the signals from the masses 66 and 128. The ratio is time independent in the first approximation.

Panel c2 shows the time dependence of the ratio of the signals from the masses 110 and 78. This ratio decrease with time. That may be the result of the increase with time of the stream of the mass 78 observed in panel b2.

The observed dependence of the particle emission magnitude for CdTe, CdSe and ZnTe on the target properties can in a large part be explained with the difference in the target heat conductance. For example, the fact that the stream intensity emitted from the N-PP target is higher than the intensities found for BC and PP targets at the same ablation conditions can be explained by the poor heat conductance of the N-PP target that leads to a local temperature increase, and finally results in a more intensive particle emission.

It is observed that for all targets, the intensity of the stream of the emitted particles is initially higher for the overlapping spots, but the intensity strongly decreases with time, and after first 3-4 minutes the intensity decreases below the level observed for the non-overlapping spots. The higher initial vapour stream intensity in the case of the overlapping spots can also be explained in terms of the local temperature increase. However, the strong decrease in the vapour intensity with time needs additional explanation. First of all, it is observed that the decrease in the vapour intensity is strictly correlated with the increase in the surface roughness. The latter is expected to result in a decrease in the angular dependence of the emitted particles. It is known that the laser ablation of a flat and smooth target surface leads to a very directional particle emission. Preferred is the "forward emission", i.e. emission in the direction normal to the surface. In the case of a rough surface the local forward emission can be directed quite differently than the direction of the normal to the target surface as a whole. Thus, it is expected that emission from a rough target will be much less directional than that from a smooth target. In such a case the number of particles reaching the QMS detector, of which the angular position is close to the target normal, will strongly decrease with the increase in the surface roughness. Therefore, it is possible that the observed decrease in the measured by QMS stream intensity is associated with the structural changes (roughness) of the target surface resulting in changes in the stream angular dependence, rather than reflects any real changes in the total stream intensity.

Cheung in his PLA studies of CdTe (Cheung, 1987) found that the stream intensity ratio $J(Te)/J(Te_2)$ strongly increases with the laser pulse power. In some qualitative agreement with that, we find that in the case of the typical thermal evaporation, this ratio increases with temperature, from a value of about 0.2 to a value of about 0.4, and ratios $J(Te)/J(Te_2$ higher than 0.5 can be reached in the typical laser ablation only. Therefore, one can assume that the increase in the ratio $J(Te)/J(Te_2)$ is a measure of a departure from the purely thermal evaporation to the typical laser ablation. In the result, one can conclude that the most typical in character pulsed laser ablation has the ablation of the BC target with no spatial overlapping of the consecutive laser shots. The steady increase in the $J(Te)/J(Te_2)$ ratio with time to the final value of 2.0 suggests that in a later time the target temperature still increases, which is equivalent to an increase in the laser pulse power. The same thermal effects can be responsible for the increase with time of the $J(Te)/J(Te_2)$ ratios for the remaining targets. The very low $J(Te)/J(Te_2)$ ratio in the case of the bulk crystal target ablated with overlapping shots can be related to a considerably larger spot overlapping (larger than in the case of the powder targets) resulting from the smaller diameter of that target. Due to the local overheating of the target, the particle emission has the chemical composition that is closer to a pure thermal evaporation than to a typical laser ablation.

3.3 Dependence on target preparation method: Summary and conclusions

The main goal of this Section is to explain the effect of the target preparation method on the ablation process. The basic investigation method is the determination of the vapour stream intensity and chemical composition, as well as their real time evolution with the help of a quadrupole mass spectrometer synchronized with the laser action. The studies are performed for three kinds of targets made of CdTe, CdSe and ZnTe. Such investigations are carried out for the first time. They revealed that the ablation has a thermal character; i. e. the process is thermally activated through an energy barrier (Kelly & Miotello, 1994). In spite of the fact that he ablation process is performed in the low power regime, it is very effective because of the high volatility of the 2-6 compounds. The thermal ablation is concluded on the basis of Fig. 3, which shows that for all compounds the stream density is proportional to the pulse energy reciprocal. Hence, the experimental results can be described by the relationship of Eq. (1), if one assumed that the thermal energy kT is gained from the laser pulse energy.

It may be observed in Fig. 3 that for CdSe and ZnTe the evaporated masses per pulse are comparable, and for CdTe they are smaller. Nevertheless, for the pulse energy of 1/6 J (=166 mJ) the emitted mass is about 1 μg/pulse for all the compounds. This means that a target prepared from a homogeneous mixture of powders of these compounds should under the laser ablation emit the vapour of chemical composition corresponding to the target average composition. Thus homogeneous thin films of mixed crystals of the compounds could be obtained.

In the PLA experiments, the target erosion is large and is characterized by a considerable surface roughness, especially in the case of the powder targets. The surface roughness increases with the laser pulse power and frequency and also with the degree of spatial overlapping of subsequent laser pulse spots on the target surface. With the development of the roughness the ablation effectiveness decreases. It seems that the apparent decrease in the particle emission is connected with a change in the angular distribution of the emitted particles introduced by the roughness. The less forward directed particle emission from the target, confirmed further on by the studies of the stream angular distribution, could be important for the practical application of PLD as a thin film deposition method because the typical very directional particle evaporation is a drawback of PLD.

In the present experiments, large surface roughness is as a rule formed in the conditions of target overheating, which results in an enhanced target vaporisation. In this case the vapour stream consists of a component typical for the true laser vaporisation and a component typical for the thermal vaporisation associated with the target overheating. These two components can be distinguished in the investigations of the ratio of the number of the monatomic VI group particles (VI = Te or Se) to the number of the diatomic particles VI_2 (Te_2., Se_2). In the case of CdTe, the stream ratio $J(Te)/J(Te_2) < 0.5$ is typical for pure thermal vaporisation and the $J(Te)/J(Te_2) > 0.5$ is typical for true laser ablation. The highest value of the ratio is found during the ablation of the CdTe BC target without any spot overlapping. Only in this case the vapour stream has the stoichiometric composition (Cd/Te = 1) from the beginning of the ablation. In the other ablation processes, the vapour stream has some excess of Cd during the first minutes of the ablation. This period can be prolonged in the ablation of the powder targets with the spot overlapping. These effects are understood in terms of the differences in the thermal conductivity between the targets.

The obtained experimental results can be a basis of a comparison of the targets from the point of view of their practical value. The most useful chemical composition of the vapour

stream in the low power regime can be obtained with the target made of a slice of a crystalline 2-6 compound ablated with well specially separated subsequent laser shots. The stream composition is in this case stoichiometric from the beginning and has a high particle ratio J(VI)/J(VI_2). The latter is advantageous for obtaining high quality epitaxial films of the 2-6 compounds (Cheung, 1987). A substantial drawback of that target, when ablated with the Nd:YAG laser, is the energetic threshold for the ablation and the (irregular) delay in the ablation process above the threshold.

On contrary, the main advantage of the powder targets over the BC target is the lack of any ablation threshold or delay. Also the costs of preparation of the powder targets are substantially lower. However, the smaller effective heat conductance of these targets poses the problem of the target overheating even in a more demanding form. To avoid the generation of the thermal component of the vapour stream, the subsequent laser shots should be well spatially separated. In addition to this, the laser frequency and/or improved heat sink may have to be applied. The target prepared from the compressed powder is a reasonable choice for the pulsed laser deposition of thin films of the 2-6 compounds, provided that the initial ablation, in which the more intense splashing and the non-stoichiometric composition of the vapour take place, is eliminated. This can be done by the use of a typical shutter that is a standard equipment of most vacuum evaporation plants.

The N-PP target is the simplest form of the target that can be prepared instantly. The main advantage of that target is that due to the very low thermal conductivity, it can be ablated effectively with very small laser powers. However, owing to the splashing, the large thermal component, and the non-stoichiometry of the vapour stream, its applicability to the pulsed laser deposition of the thin films of the II-VI compounds is rather limited to some preliminary deposition tests.

4. Pulsed laser ablation of 2-6 compounds: Velocity distribution of emitted particles

In this section we continue the investigation of the ablation process through the determination of the emitted particle velocity and angle distribution. The velocity distribution is determined by the time-of-fly spectrometry. It is known that the TOF spectrometry is a very useful characterisation method of the PLA process; however, the interpretation of results obtained needs a lot of care (Kelly & Miotello, 1994).

The information on the distribution of particle velocities during the laser ablation of the 2-6 compounds is rather limited. The PLA of CdTe was performed by Cheung (Cheung, 1987). He used 100 μm pulses of a Nd:YAG laser and found that the particle velocity distribution is the full Maxwell-Boltzmann. Namiki et al. (Namiki et al., 1986) also observed the full M-B distribution of particles for CdS. However, as shown further on, our velocity distributions obtained from the TOF studies are much narrower than the classic M-B distribution, which means that ablation takes place in the condition of the formation of the Knudsen layer (KL) followed by adiabatic expansion (KL-AE). These studies are carried out for all three types of targets and from them the velocities of the stream and the most probable velocities in the centre-of-mass system are determined.

The formation of KL-AE leads to a specific angular distribution of the emitted particles, which is strongly forward directed. The investigation of those distributions for the three types of the target is also the subject of our studies.

4.1 Theoretical velocity distribution

The laser ablation process, in particular PLA, of various solid state materials both organic and inorganic, liquids and suspensions is a point of interest for many researchers working in a wide variety of scientific domains. This diversity may be the reason of the existing confusion on the nomenclature, definitions and assumptions encountered in the literature devoted to the physical description of the gas (plasma) generated in vacuum by laser pulses. In this connection, it seems appropriate to introduce the definitions and formulae that are used in the presentation and interpretation of the experimental results presented in the further part of this contribution.

The velocity distribution of a perfect gas at temperature, T is described by the Maxwell-Boltzmann distribution function

$$f(v) \propto v^2 \exp\left(-\frac{v^2}{v_0^2}\right) \tag{2}$$

where v is the particle velocity and

$$v_o = \sqrt{2kT/m}\,, \tag{3}$$

is the most probable particle velocity in the gas. In Eq. (3), T is the gas temperature, and m is the particles mass. In the Cartesian coordinate system, in which the gas mass centre is resting, $v^2 = v_x^2 + v_y^2 + v_z^2$, and $-\infty < v_x, v_y, v_z < +\infty$. The same functional form has the velocity distribution of particles emitted during the thermal ablation of a target, provided that the particle concentration is sufficiently small for the emission process to be collisionless (Kools et al., 1992; Anisimov, 1968). If the target normal is directed along the z-axis, the movement along this direction is limited by the condition, $v_z > 0$, which means that the centre-of-mass of the particle stream drives away from the target surface. Therefore, the gas is described by the distribution defined by Eq. (2) with $v_z > 0$. This so-called "half-range" M-B distribution can be the basis of the interpretation of the TOF measurements, provided that the following measurement conditions are fulfilled (Kelly & Dreyfus, 1988):

a. Both the detector sensitive area and the emission area are small in comparison with the distance between them,
b. The detector is on-axis, i.e., the detector area and the emission area are parallel and have a common normal,
c. The particle emission time is much smaller than TOF.

The specific geometry of TOF measurements causes the TOF distribution is different from that given by Eq. (2) by a pre-exponential factor v^n. In the case of the TOF distribution we have

$$f_{\mathrm{TOF}}(v) \propto v^4 \exp\left(-\frac{v^2}{v_0^2}\right). \tag{4}$$

It should be mentioned that this form of the TOF distribution function with $n = 4$ applies to the particle detector sensitive to particle concentration. This is the case when a QMS is applied (Kelly & Dreyfus, 1988). The v in Eq. (4) is the velocity measured within a small solid angle around the target surface normal, i. e., $v \cong v_z$.

It is sometimes argued that the pre-exponential factor in Eq. (4) should be v^3 (Kools et al., 1992) instead of v^4. We are, however, more convinced by the arguments given by Kelly (Kelly, 1992) for the pre-exponential factor v^4, and will thus use it in the following. However, in view of the dominant role of the exponential term, the difference between those two pre-exponential factors does not have any meaningful effect on the general interpretation of the presented experimental results.

Particle emission with collisions is accompanied by the formation of the Knudsen layer at the target surface, where the collisions occur. In such a case, Eq. (2), with the condition, $v_z > 0$, applies at the closest vicinity of the target surface only. Moreover, owing to the collisions, the gas cloud evolves to the distribution called *shifted M-B* or *M-B on stream velocity*. In this distribution v_z in Eq. (2) has to be replaced by $(v_z - u)$, where u is the so-called *stream velocity* or *centre-of mass-velocity*. In the result, when the Knudsen layer is formed one obtains:

$$f(v) \propto v^2 \exp\left(-\frac{(v-u)^2}{v_0^2}\right). \tag{5}$$

It is important to note that, owing to collisions, for this distribution we have: $-\infty < v_x, v_y, v_z < +\infty$. For $u = 0$, we are in the COM system, and the distribution becomes the classic M-B distribution of Eq. (2). Now, v_0 is the most probable velocity among the velocities, v in the COM system, and Eq. (3) defines temperature in the COM system. In the laboratory system, to the distribution described by Eq. (5) belongs the following most probable velocity:

$$v_{0,r} = \frac{u}{2} + \sqrt{\left(\frac{u}{2}\right)^2 + v_0^2}\ . \tag{6}$$

It is observed that for $u >> v_0$, from Eq. (6) one obtains $v_{0,r} \cong u$.

With the formation of the Knudsen layer, Eq. (4) evolves to the form

$$f_{\mathrm{TOF}}(v) \propto v^4 \exp\left(-\frac{(v-u)^2}{v_0^2}\right). \tag{7}$$

Again, v is the velocity measured within a small solid angle around the target surface normal ($v \cong v_z$), and v_0 is given by Eq. (3). From the extremum condition for this distribution function, one obtains the following most probable velocity in the laboratory system:

$$v_{0,TOF} = \frac{u}{2} + \sqrt{\left(\frac{u}{2}\right)^2 + 2v_0^2} \tag{8}$$

Since for $u = 0$, Eq. (5) reduces to Eq. (4), where v_0 is the most probable velocity of the classic M-B distribution in the COM coordinate system.

For very high density of emitted particles, the number of collisions in the KL increases leading to the adiabatic expansion. In that case the velocity distribution is still described by Eq. (5) (Kools et al., 1992). However, it becomes more "narrow", i. e. its FWHM decreases.

4.2 Experimental velocity distribution and its comparison with theoretical predictions

The reliability of the obtained TOF experimental data depends on the fulfilment of the conditions (a)-(c) listed in Sec. 4.1. In an earlier paper (Rzeszutek et al., 2008b) it was shown that the described in Sec. 2.2 equipment for TOF measurements fulfils the conditions. Thus the equations of Sec. 4.1 are applicable to the interpretation of the performed TOF experiments.

The TOF measurements are performed for all atomic and diatomic species emitted from the investigated targets. In the case of CdTe the TOF measurements are carry out for all three sorts of target, and in the case of CdSe and ZnTe they are carry out on PP targets only.

The measurement results of the TOF velocity distribution for a CdTe BC target ablated with 220 mJ laser pulses are shown in Fig. 10.

The solid lines being theoretical fits to experimental points are obtained with the use of Eq. (7). The theoretical curve fits in Fig. 10, as well as those in Figs. 11–13 are performed with the computer application Origin 7.0 with the option of the least squares method. The values of the velocities u and v_0 obtained from those fitting are given in the inserts to the figures. In

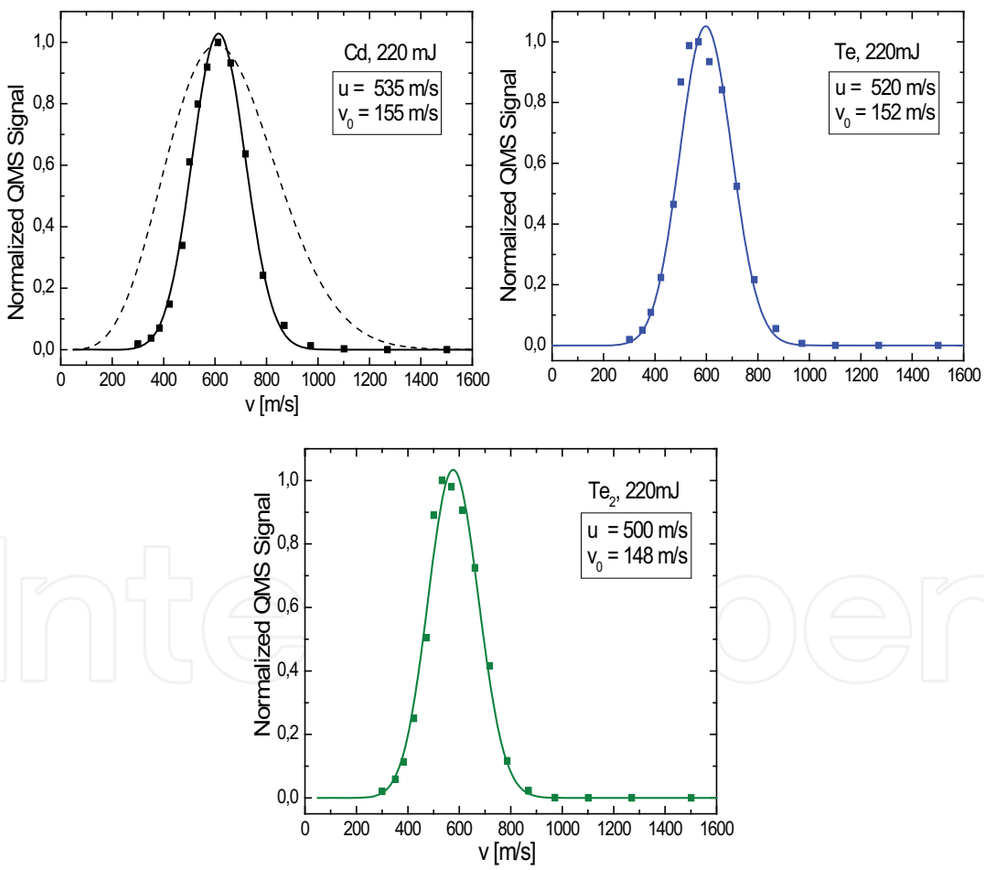

Fig. 10. TOF velocity distributions for atoms of Cd and Te and diatomic molecules, Te_2. Results are for CdTe BC target ablated with 220 mJ laser pulses with frequency of 25 Hz. Solid curves are obtained from theoretical fit to the experimental points with help of Eq. (7). Fitting parameters u and v_0 are given in inserts. For Cd fit with Eq. (4) is also made and shown as dashed curve for comparison.

the case of Cd, the fit with $u = 0$ is also given for comparison. This is in effect a fit to the TOF distribution of the classic M-B distribution (Eq. (4)). It is clear from the comparison that the experimental distributions are rather narrow, and thereby have to be described by the TOF shifted M-B distribution (Eq. (7)). It is seen in Fig. 10 that the fit with Eq. (7) is rather good, and therefore the values of the velocities u and v_0 are determined with a fairly good accuracy. The description of the experimental distributions with Eq. (7) means that the Knudsen layer is formed, hence the particles encounter collisions.

The velocity distribution for the CdTe PP target is determined for two laser pulse energies: 280 mJ and 160 mJ. The results are shown in Fig. 11.

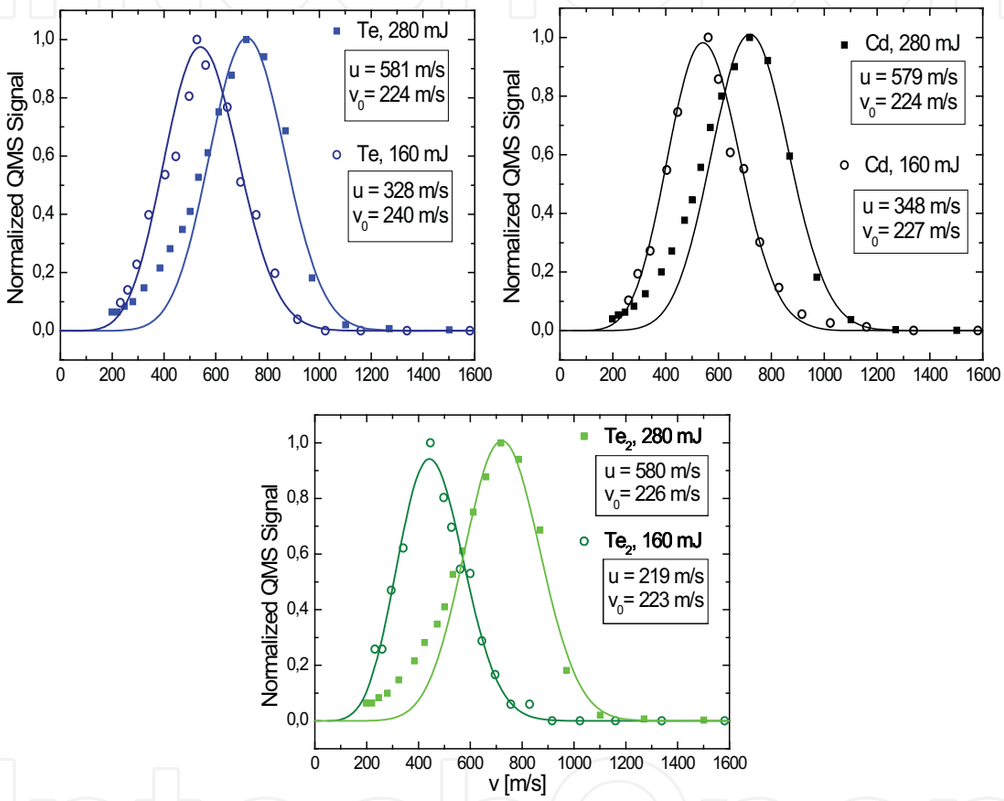

Fig. 11. TOF velocity distributions for atoms of Cd and Te and diatomic molecules Te_2. Results are for CdTe PP target ablated with 280 mJ and 160 mJ laser pulses of 25 Hz frequency. Solid curves are obtained from theoretical fit to experimental points with the help of Eq. (7). Fitting parameters u and v_0 are given in the inserts.

It is seen that the velocity distributions for the 280 mJ pulses are shifted to higher velocities, as may be expected. It is also observed that the theoretical fit to the experimental points is generally good, with the exception of the low velocity side for the 280 mJ pulses. The existence of the "low velocity tail" for the 280 mJ pulses can be ascribed to the target overheating, which results in the emission of the low energy particles of the heat origin, as described in Sec. 3. In the case of the 280 mJ pulses we observe, as in the BC target case, a close similarity between all particle distributions, leading to very close values of the most probable velocity. On contrary, in the case of 160 mJ pulses, the most probable velocity of the diatomic molecules is clearly smaller than those of the monatomic particles.

The results of the TOF velocity distribution measurements for the CdTe N-PP target ablated with 160 m J pulse energies are shown in Fig. 12.

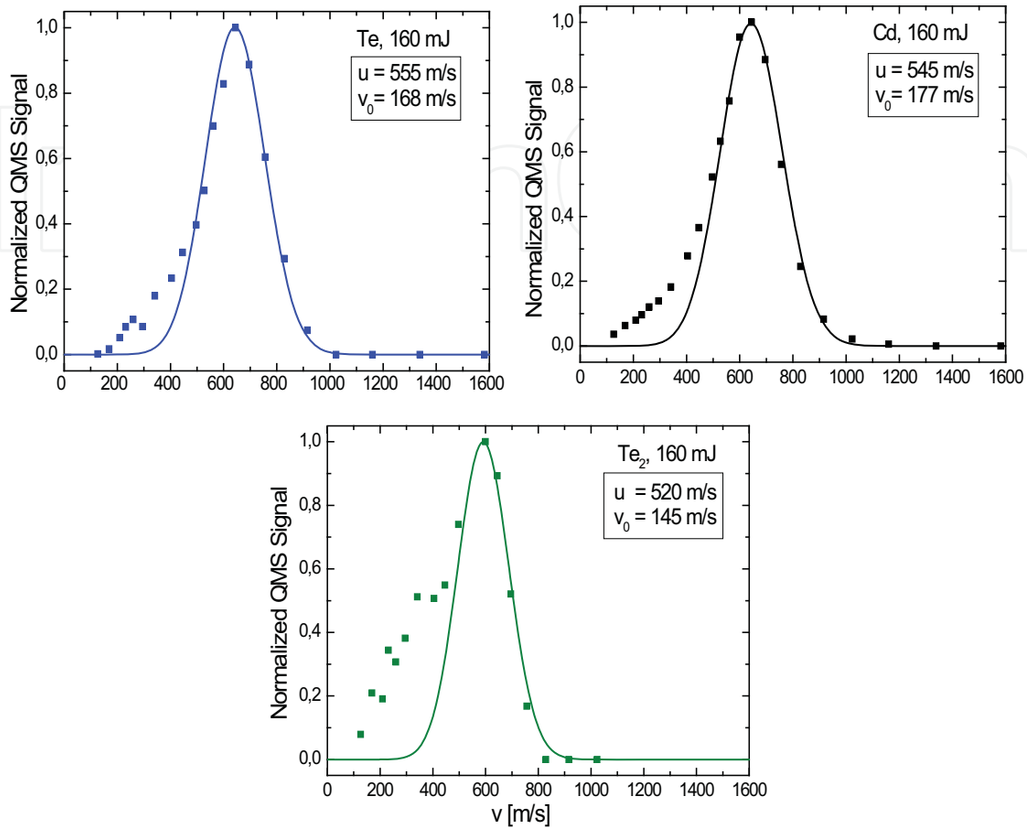

Fig. 12. TOF velocity distributions for atoms of Cd and Te and diatomic molecules Te_2. Results are for CdTe N-PP target ablated with 160 mJ laser pulses of 25 Hz frequency. Solid curves are obtained from theoretical fit to experimental points with the help of Eq. (7). Fitting parameters u and v_0 are given in the inserts.

It may be seen that even for this relatively small pulse energy, the velocity distributions are affected by the low temperature tail. This low temperature tail is particularly clearly observed in the case of Te_2 molecules. This may be understood, because the Te_2 diatomic molecules are larger in number than the monatomic Te in the particle stream emitted thermally from an overheated target. The distributions for the CdTe N-PP target are similar to those of CdTe PP target of the CdTe PP target ablated with 280 mJ pulses. This means that due to a smaller thermal conductivity of the CdTe N-PP target, the effective temperature of the target ablation is for that target higher. This also confirms the conclusion of Sec. 3 that at the same laser pulse energy the effectiveness of the laser ablation of a N-PP target is higher in comparison with a PP target.

The TOF velocity distributions for CdSe and ZnTe are measured for PP targets with 160 mJ laser pulse energies and the frequency of 25 Hz. They are shown in Fig. 13.

Like in the case of the CdTe PP target, the particle velocity distributions for CdSe and ZnTe are narrow and show "the low velocity tail", which is more clearly seen for ZnTe. Therefore, the general features of the distributions are dependent on the compound chemical composition.

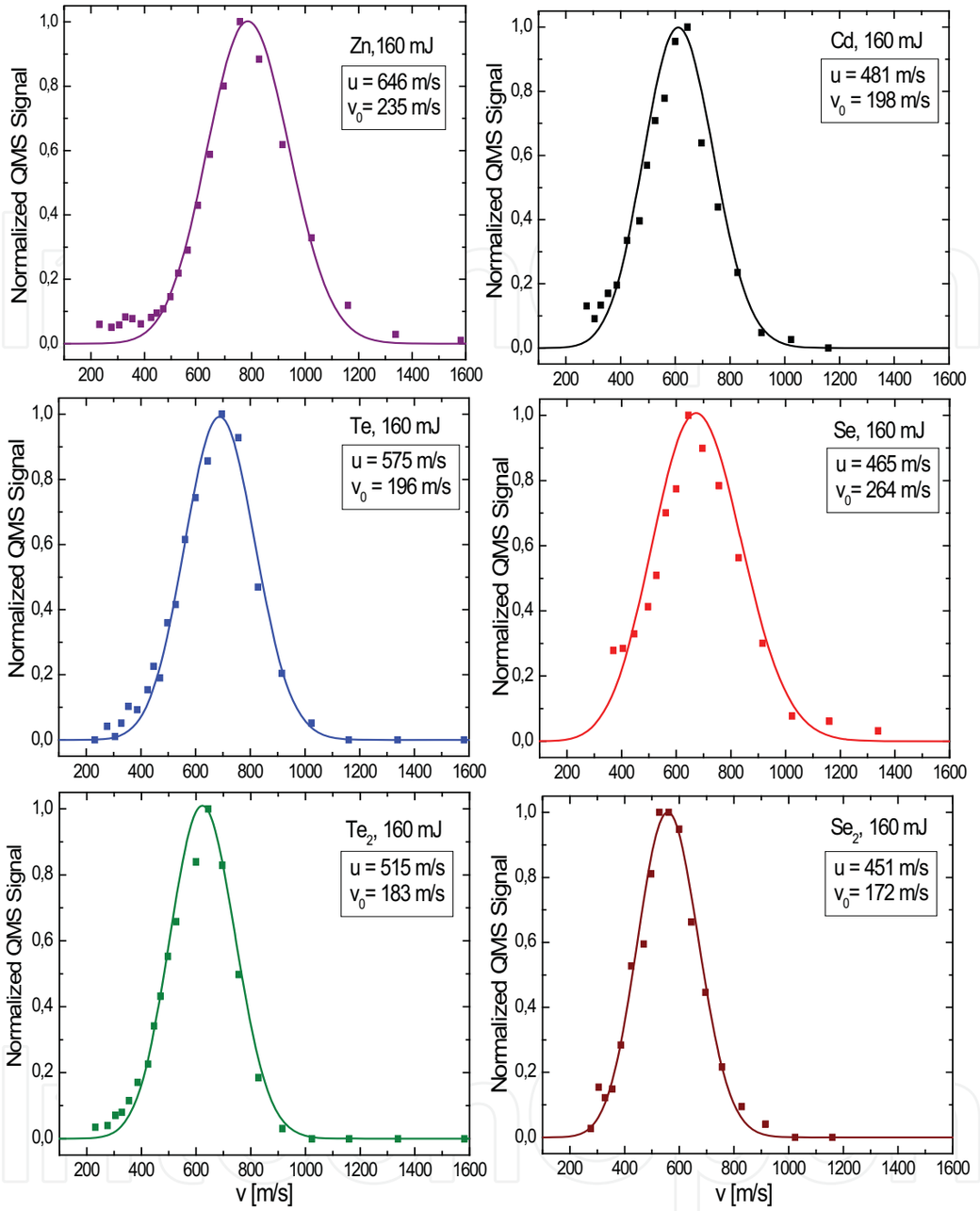

Fig. 13. TOF velocity distributions for CdSe PP and ZnTe PP targets ablated with 160 mJ laser pulses of frequency of 25 Hz Solid curves are obtained from theoretical fit to experimental points with the help of Eq. (7). Fitting parameters u and v_0 are given in the inserts.

4.3 Particle velocity distribution: Discussion and conclusions

In the present studies is observed substantial narrowing of the velocity distributions for all types of targets. The physical parameters of the gas phase, as determined form the best fit of the data in Figs. 10 – 13, are compiled in Table 1.

Target	energy pulse [mJ]	particle	v_0 [m/s]	u [m/s]	c [m/s]	T [K]	$v_{0,r}$ [m/s]	T_r [K]	M [–]
		Cd	155	535	141	159	577	2200	3.8
BC,	220	Te	152	520	139	178	561	2424	3.7
CdTe		Te_2	148	500	135	337	541	4499	3.7
		Cd	224	579	204	332	656	2843	2.8
PP,	280	Te	224	581	204	386	657	3326	2.8
CdTe		Te_2	226	580	206	786	658	6660	2.8
		Cd	227	348	207	341	460	1400	1.7
PP,	160	Te	240	328	215	443	455	1592	1.5
CdTe		Te_2	223	219	311	766	358	1973	0.7
		Cd	177	545	162	207	597	2361	3.4
N-PP	160	Te	168	555	153	217	602	2789	3.6
CdTe		Te_2	145	520	132	324	558	4789	3.9
		Zn	235	646	215	219	722	2072	3.0
PP,	160	Te	196	575	179	296	635	3109	3.2
ZnTe		Te_2	183	515	167	516	573	5062	3.1
		Cd	198	481	181	259	552	2016	2.7
PP,	160	Se	264	466	241	327	585	1606	1.9
CdSe		Se_2	172	451	157	278	509	2432	2.9

Table 1. Particle stream parameters emitted from various targets.

The first column in the table shows the target preparation method and material, the second column gives the energy of the laser shot at which the target was ablated, and the third column specifies the emitted particles. The fourth and the fifth columns present respectively the values of the most probable particle velocity v_0 in the frame of COM system and the COM velocity, u in the laboratory system. In the eighth column values of most probable velocity in the laboratory system $v_{0,r}$ are given. If $u > v_0$ as it is in the present case, the most probable velocities given by Eqs. (8) and (6) are rather close. In the present case, $v_{0,r}$ is smaller than $v_{0,\mathrm{TOF}}$ by about 20%. This may be verified by comparing the values of $v_{0,r}$ in the table with the values of $v_{0,\mathrm{TOF}}$ read out from the distribution maxima in Figs 10 – 13. We prefer to present in the table the values of $v_{0,r}$ because they are not directly associated with the measurement method (TOF).

To $v_{0,r}$ one can formally ascribe temperature T_r according to the equation analogous to the relationship described by Eq. (3):

$$kT_r = \frac{mv_{0,r}^2}{2}, \tag{9}$$

where T_r is a certain measure of the average kinetic energy, in the laboratory system, of particles subjected to the adiabatic expansion. Because it describes the gas phase after its

thermalization in the collisional process, T_r is smaller than the target surface temperature (Kools et al., 1992) The calculated values of T_r are shown in the ninth column. It may be seen that for each 2-6 compound, irrespective of the target preparation method, T_r increases with the particle mass, which means that the emitted particles form independent energetic systems.

The values of the most probable velocities v_0 in the COM system are considerably smaller than the values of $v_{0,r}$. The temperatures in COM system calculated from these values of v_0, obtained by using Eq. (3) are displayed in the seventh column of the table. It may be seen that they are generally low, and can be even lower than room temperature. To these temperatures can be ascribed sound velocity, c according to the classic rule applicable to perfect gas:

$$c = \sqrt{\gamma kT / m} = v_0 \sqrt{\gamma / 2}\ , \tag{10}$$

where $\gamma = (j+5)/(j+3)$ is the specific heat ratio (adiabatic index) for perfect gas, and j is the number of internal degrees of freedom accessible at T. For the monatomic species, j = 0, and for the diatomic species maximum j = 3. The values of the sound velocities are given in the sixth column of the table. For the diatomic particles we present data for j = 0 as the number of occurring degrees of freedom in the present experimental conditions is not known. In the last column we present the expansion Mach number $M = u/c$, which is the measure of the velocity distribution narrowing.

Table 1 reveals the following interesting trends in the behaviour of the emitted particles:

1. The velocity $v_{0,r}$ depends on the pulse energy and the target material and preparation method. For the CdTe PP target, the velocities are higher for 280 mJ pulses than for 160 mJ pulses. On the other hand, for 160 mJ pulses, the values of $v_{0,r}$ are higher for the CdTe N-PP target than those for the CdTe PP target. This is obviously due to the smaller thermal conduction of the N-PP target resulting in higher evaporation temperature. In turn, the values of $v_{0,r}$ for the N-PP target are comparable with those of the BC target, in spite of the smaller pulse energy of the former. This is also due to the difference in the thermal conduction of the targets.
2. In general, for a given target material and preparation method the values of $v_{0,r}$ for monatomic and diatomic particles are comparable Nevertheless, some differences in the dependence on the mass can be noted. For example, for a smaller effective pulse energy (the case of CdTe BC and CdTe PP-160 mJ), the velocity $v_{0,r}$ decreases with the mass and for higher effective pulse energy (the case of CdTe PP-280 mJ), the velocity $v_{0,r}$ becomes roughly independent of the mass. The case of CdTe N-PP target does not follow that rule, which may be associated with a disturbance in the TOF spectrum by the thermal component of particles in the Te_2 stream. Among the PP targets ablated with 160 mJ laser pulses the highest values of $v_{0,r}$ shows the ZnTe target, and smaller values shows CdTe target.
3. One could expect that as v_0 is the most probable velocity in COM system, described by the classic M-B distribution, the most probable velocity, v_0 of various species will scale with the mass in the same way as it occurs in the perfect gas, that is as $m^{-0.5}$. This is obviously based on the assumption that temperature T is the same for all species. Actually, as may be seen in the table, the velocities for the same ablation process do, in general, decrease with the mass, but the decrease is considerably smaller than that described by the $m^{-0.5}$ dependence. This generally weaker mass dependence seems to

show that the multicomponent gas does not attain the thermal equilibrium in COM system. This presumably occurs because of an insufficient number of collisions. The lack of equilibrium reflects temperature T that increases with the increase in mass. That means that different species form different energetic subsystems.

4. The COM velocity *u* shows a weak dependence on the particle mass, with the exception of the CdTe PP target ablated with 0.16 J pulses. For the same ablation conditions, the value of *u* decreases with mass for less energetic particles, and becomes nearly independent of mass for more energetic particles. A clear example of this behaviour is the result obtained for the CdTe PP target ablated with 160 mJ and 280 mJ pulses. Therefore, it is observed that for a more energetic ablation, the levelling of the value of the COM velocity *u* takes place for all masses.

With the exception for the CdTe PP target ablated with 160 mJ pulses, for which M considerably decreases with mass, the Mach numbers weakly depend on the mass. Since M is a measure of the degree of the stream forward directionality and increases with the number of collisions, it is understood that the Mach numbers are higher in the case of the CdTe PP target ablated with 280 mJ pulses than in the case of the same target ablated with 160 mJ pulses. However, it is not clear why the Mach numbers of PP target ablated with 280 mJ pulses are smaller than those of CdTe BC and CdTe N-PP targets. The Mach numbers for the ZnTe PP target are high, and those for the CdSe are smaller.

The peculiarities of the velocity distributions observed in our experiments and their comparison with the data published for materials other than the 2–6 compounds (Rzeszutek et al., 2008b) show that the stream behaviour is governed by a number of ablation parameters. Unfortunately, our results cannot be compared with results obtained by other researchers for 2–6 compounds, because publications on such data practically do not exist. Nevertheless, it seems to be clear from the available data that the number of collisions prior to the gas expansion plays an important role, especially in the process of levelling the stream velocities for different masses. It should be pointed out that the velocity levelling has no satisfactory theoretical explanation yet. This is obviously due to the complexity of the processes occurring in the gas phase. Kelly and Dreyfus (Kelly & Dreyfus, 1988) suggest that in a two-component system the levelling may take place due to the formation of KL at the solid-gas boundary.

In view of the lack of any detailed interpretation of the velocity equalization, it may be worthy to consider a similar effect in the mesoscopic scale that takes place in the matrix-assisted laser ablation of molecular solids. In this technique, large molecules called the analytes are incorporated into a matrix of much smaller, but still large molecules that readily absorb the incident laser ablation.

Computer simulations performed with the molecular dynamics method show that the ablation of such molecular systems reproduces most of the characteristic features that are observed in the laser ablation of the typical solids (Zhigilei, et al., 1998; Zhigilei et al., 2003). This includes the fluence threshold for ablation, cluster formation, and the velocity distribution, in particular the forward peaking and the levelling. As for the latter, it is interpreted as a simple entrainment of the large molecules by the matrix molecules in the stream. Thus, it is the model of dragging suspended particles in flowing fluid. If this model were adopted to the microscopic scale of the small molecules and atomic species, most of the above discussed peculiarities of the velocity distribution could be explained. In particular, for sufficient fluence that results in a large number of collisions in the gas phase, the larger

particles with larger masses have to be entrained and thereby they level their velocities to the common stream velocity.

4.4 Angular distribution of particles

Particle emission with velocity distribution described by Eq. (7) is expected to be strongly forward directed (Saenger, 1994). In this respect, the measurements of the angular distribution of the particles are auxiliary to TOF measurements.

For the determination of the angular distribution we use a typical method of measuring the profile of a deposited thin film. For this purpose, glass plates are glued with liquid indium to the surface of the circular substrate heater, shown schematically in Fig. 2 by the dotted lines. The substrate plates are aligned along several concentric circles that are centred vertically above the laser spot on the target. The film thickness is measured with an interference optical microscope. This measurement procedure is described in more detail in (Rzeszutek et al., 2008b).

Having determined the distribution of the film thickness along the radius, the dependence of the film thickness on the polar angle θ can be obtained. Such dependence for all kinds of the CdTe targets ablated with 160 mJ laser pulses with frequency of 35 Hz is shown in Fig. 14.

For the interpretation of the experimental results, it is assumed that the theoretical dependence of the film thickness d on θ is of the form (Saenger, 1994):

$$d = d_0 \cos^m \theta \tag{11}$$

where d_0 is the thickness in the circle centre, i. e. corresponding to $\theta = 0$. The dependence of the relative film thickness d/d_0 on θ, predicted by Eq. (11) for several values of m is shown in Fig. 14.

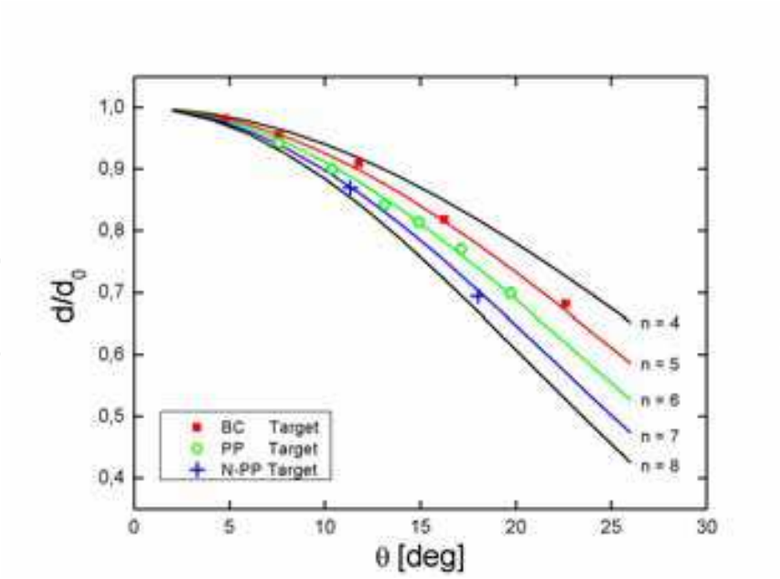

Fig. 14. Dependence of the relative film thickness d/d_0 on the polar angle θ for the three kinds of CdTe targets. Solid lines show the dependence predicted by Eq. (11) for various values of the exponent m. The values of d_0 for BC, PP and N-PP targets respectively are: 1.1 μm, 0.7 μm and 1.5 μm.

Comparing the experimental point with the theoretical curve we obtain the value of the exponent *m*. It is seen that the experimental points for CdTe BC target match with the curve obtained for *m* = 5, the experimental points for CdTe PP target are in agreement with the curve obtained for *m* = 6, and the experimental points for CdTe N-PP target are well described by the curve obtained for *m* = 7. It appears that the increase in the exponent *m* is correlated with the stream intensity, which is the less intense for BC target, and is the most intense for N-PP target.

Similar angular distribution of particles is determined for CdSe PP and ZnTe PP targets. In these experiments the energy of laser pulses is 160 mJ and the pulse frequency is 25 Hz. The result is that the exponent in Eq. (11) is m = 6. Thus, independent on material, the ablation of a PP target leads to the value of m = 6.

The investigations of the stream angular dependence show that the results are well described by Eq. (11) with *m* > 4. The value of 4 corresponds to the evaporation from a Knudsen cell and also from a flat target with no collisions in the gas phase. The obtained values *m* = 5 - 7 are considerably smaller than those expected for very forward-directed laser ablation with number of collisions in the gas phase (Saenger, 1994). A possible explanation of the small values of the exponent is the roughness of the target arising in the ablation process. High values of the exponent corresponding to very forward–directed evaporation are possible only for flat targets.

5. Final conclusions

Results of the investigations of the laser ablation of CdTe, CdSe and ZnTe with pulsed Nd:YAG laser are presented. They are performed with 100 μs pulses having energy from 130 mJ to 280 mJ. The laser pulses fall into the low power regime that allows diminishing effectively the splashing effect. The main goal of the studies is to elucidate the ablation process dependence on the target preparation method and the pulse energy.

The main investigation method is the determination of the vapour stream intensity and chemical composition, as well as their real time evolution with the help of a quadrupole mass spectrometer synchronized with the laser action. The studies are performed for three kinds of targets: target cut from crystalline CdTe, target made of powdered material formed into a pellet under high pressure and target made of loose powder.

The investigation reveals that the ablation has a thermal character and is very effective in this low power regime, due to the high volatility of the 2-6 compounds. The target erosion is large and is characterized by a considerable surface roughness, especially in the case of the powder targets. The surface roughness increases with the laser pulse power and with the degree of spatial overlapping of subsequent laser pulse spots on the target surface. With the development of the roughness, the ablation effectiveness, as measured by the quadrupole mass spectrometer strongly decreases. The decrease in the particle emission is apparently connected with a change in the angular distribution of the emitted particles introduced by the roughness. The less forward directed particle emission from the target is confirmed in the further investigations.

A large surface roughness is formed in the conditions of target overheating that results in intensive target vaporisation. In such a case the vapour stream consists of a component typical for the true laser vaporisation and a component typical for the thermal vaporisation associated with the target overheating.

The obtained experimental results can be a basis of a comparison of the targets from the point of view of their practical value. The best chemical composition of the vapour stream for obtaining high quality thin films can be obtained for a target made of a bulk crystal (BC) ablated with non-overlapping laser spots. A substantial drawback of that target, when ablated with the Nd:YAG laser, is an energetic threshold for the ablation and a delay in the ablation process

The main advantage of a pressed powder (PP) target over a BC target is the lack of any ablation threshold or delay. Also the costs of preparation of a PP target is substantially lower. However, the smaller effective heat conductance of the PP targets poses a problem of the target overheating. To avoid the generation of the thermal component of the vapour stream, the subsequent laser shots should be well spatially separated.

Mass spectrometer TOF measurements of the particle velocity distributions revealed their substantial narrowing, i. e. decrease in the FWHM of the distribution curves. The velocity distributions are well described by the shifted M-B distribution, of which parameters are: the stream velocity u in the laboratory system and the most probable velocity v_0 in the centre-of-mass (stream) system. According to the existing theory, with increase in the number of collisions in the gas phase, the half-range M-B distribution describing the collisionless gas phase evolves into the shifted M-B distribution. The available experimental data computer simulations, suggest that this should also be true for multicomponent gases consisting of several sorts of particles having different masses. This means that on reaching thermodynamic equilibrium, all the particles should form a common system having the same u, and v_0 should scale with particle mass as $m^{-0.5}$. However, our measurements show that at lower pulse energies the values of u decrease with particle mass, but with energy increase the values of u level. For the explanation of the velocity levelling, we adopt a model emerging from the matrix-assisted laser ablation of molecular solids computer simulation (Zhigilei et al.,1998; Zhigilei et al., 2003). In this model, the larger masses having smaller concentration are entrained into the stream of the smaller masses and hence level their velocities to a common stream velocity.

In our experiments the stream velocities are in the range 220÷650 m/s and the most probable in the centre-of-mass velocities are in the range 140÷240 m/s. The velocity in the laboratory system, which is 450÷700 m/s depends both on the laser pulse energy and the target preparation method. The dependence on the target preparation clearly results from the difference in their heat conductivities. Higher heat conductivity leads to higher effective temperature of evaporation and thereby to higher particle velocities. The highest heat conductivity has the bulk crystal target.

The obtained from the measurements angular dependence of the stream is smaller than expected. It seems to be associated with the roughness of the target arising in the ablation process. The confirmation of the relatively weak angular dependence is important for practical reasons, because it is the strong angular dependence that is characteristic for the laser ablation that causes difficulties in obtaining thin films with uniform thickness on large substrate surfaces.

Therefore, the present studies show that the use of the YAG:Nd laser in the low power regime should be an effective preparation method of stoichiometric 2-6 compound thin films.

6. References

Anisimov, S. I. (1968). Vaporization of Metal Absorbing Laser Radiation. *Soviet Phys. JETP* 27, 182–183

Bardi, G.; Jeronimakis, K.; Trionfetti, G. (1988). Vaporization enthalpy of cadmium selenide and telluride obtained by vapor pressure measurements. *Termochim. Acta* 129, 341 – 343

Cheung J. T. (1987). Role of atomic tellurium in the growth kinetics of CdTe (111) homoepitaxy. *Appl. Phys. Lett*, 51, 1940–1942

Cheung J. T. &.Sankur, H. (1988). Growth of thin film by laser-induced evaporation. *Critical Rev. Solid St. Mat. Sci.* 15,1, 63–109

Chrisey, D. B. & Hubler, G. K. (1994). *Pulsed Laser Deposition of Thin Films*, John Wiley & Sons, New York

Dubowski, J. J. (1991). Pulsed laser evaporation and epitaxy. *Acta Phys. Polon.,* A80, 221-244

Ignatowicz, S. &. Koblendza, A. (1990). *Semiconducting Thin Film of $A^{II}B^{VI}$ Compounds*, pp. 30-37, 73, 74, PWN, Warszawa

Kelly, R. & Dreyfus, R. W. (1988). On the effect of Knudsen-layer formation on studies of vaporization, puttering and desorption. *Surf. Sci.*. 198, 263–276

Kelly, R. (1992). Gas dynamics of the pulsed emission of a perfect gas with applications to laser sputtering and to nozzle expansion. *Phys. Rev*. A46, 860–874

Kelly, R. & Miotello, A. (1994).Mechanisms of Pulsed Laser Sputtering, *In: Pulsed Laser Deposition of Thin Films* , Chrisey, D. B. & Hubler, G. K., 55-85, John Wiley & Sons, New York

Kools, J. C. S.; Baller, T. S.; De Zwart, S. T .& Dieleman, J. (1992). Gas flow dynamics in laser ablation deposition. *J.Appl. Phys.,* 71, 4547–4556

Namiki, A.; Kawi, T.& Chige, I. (1986). Angle-resolved time-of-flight spectra of neutral particles desorbed from laser irradiated CdS. *Surf. Sci.*, 166, 129–140

Nasar, A. & Shamsuddin, M. (1990). Thermodynamic properties of ZnTe. *J. Less Common Met.*, 161, 93–99

Oszwałdowski, M.; Berus, T.; Sydorczuk, P. & Rzeszutek, J. (2003). Apparatus for pulsed laser deposition of semiconductor thin films. *Review of Scientific Instruments*, 74, 3160–3163

Rzeszutek, J.; Oszwaldowski, M. &. Savchuk, V. (2008). Ablation of CdTe with 100μs Nd:YAG laser pulses: dependence on target preparation method. *Cryst. Res. Technol.* 43, 1, 32-43

Rzeszutek, J.; Oszwaldowski, M. & Savchuk, V. (2008b). Ablation of CdTe with 100μs pulses from Nd: YAG laser: Velocity distribution of emitted particles. *Nucl. Instr. And Meth*. 266, 4766–4774

Saenger, K. L. (1994).Angular Distribution of Ablated Material, *In: Pulsed Laser Deposition of Thin Films* , Chrisey, D. B. & Hubler, G. K., 199–225, John Wiley & Sons, New York

Zhigilei, L. V.; Kodali, P. B. S. & Garrison, B. J. (1998). A microscopic view of laser ablation. *J. Phys. Chem*. B, 102, 2845–2845

Zhigilei, L. V.; Leveugle, E.; Garrison, B. J.; Yingling, Y. G. & Zeifman, M. I. (2003). Computer simulations of laser ablation of molecular substrates. *Chem. Rev*. 103, 321–348

Laser Pulse Phenomena and Applications
Edited by Dr. F. J. Duarte

ISBN 978-953-307-405-4
Hard cover, 474 pages
Publisher InTech
Published online 30, November, 2010
Published in print edition November, 2010

Pulsed lasers are available in the gas, liquid, and the solid state. These lasers are also enormously versatile in their output characteristics yielding emission from very large energy pulses to very high peak-power pulses. Pulsed lasers are equally versatile in their spectral characteristics. This volume includes an impressive array of current research on pulsed laser phenomena and applications. *Laser Pulse Phenomena and Applications* covers a wide range of topics from laser powered orbital launchers, and laser rocket engines, to laser-matter interactions, detector and sensor laser technology, laser ablation, and biological applications.

How to reference
In order to correctly reference this scholarly work, feel free to copy and paste the following:

Maciej Oszwaldowski, Janusz Rzeszutek and Piotr Kuswik (2010). Ablation of 2-6 Compounds with Low Power Pulses of YAG:Nd Laser, Laser Pulse Phenomena and Applications, Dr. F. J. Duarte (Ed.), ISBN: 978-953-307-405-4, InTech, Available from: http://www.intechopen.com/books/laser-pulse-phenomena-and-applications/ablation-of-2-6-compounds-with-low-power-pulses-of-yag-nd-laser

INTECH
open science | open minds

InTech Europe
University Campus STeP Ri
Slavka Krautzeka 83/A
51000 Rijeka, Croatia
Phone: +385 (51) 770 447
Fax: +385 (51) 686 166
www.intechopen.com

InTech China
Unit 405, Office Block, Hotel Equatorial Shanghai
No.65, Yan An Road (West), Shanghai, 200040, China
中国上海市延安西路65号上海国际贵都大饭店办公楼405单元
Phone: +86-21-62489820
Fax: +86-21-62489821

IntechOpen